A&A 516, A56 (2010)
DOI: 10.1051/0004-6361/201014321
© ESO 2010

Astronomy & Astrophysics

Multi-wavelength observations of H 2356–309

HESS Collaboration, A. Abramowski[4], F. Acero[15], F. Aharonian[1,13], A. G. Akhperjanian[2], G. Anton[16], U. Barres de Almeida[8,⋆], A. R. Bazer-Bachi[3], Y. Becherini[12], B. Behera[14], W. Benbow[1,⋆⋆], K. Bernlöhr[1,5], A. Bochow[1], C. Boisson[6], J. Bolmont[19], V. Borrel[3], J. Brucker[16], F. Brun[19], P. Brun[7], R. Bühler[1], T. Bulik[29], I. Büsching[9], T. Boutelier[17], P. M. Chadwick[8], A. Charbonnier[19], R. C. G. Chaves[1], A. Cheesebrough[8], J. Conrad[31], L.-M. Chounet[10], A. C. Clapson[1], G. Coignet[11], L. Costamante[1,33,⋆⋆⋆], M. Dalton[5], M. K. Daniel[8], I. D. Davids[22,9], B. Degrange[10], C. Deil[1], H. J. Dickinson[8], A. Djannati-Ataï[12], W. Domainko[1], L. O'C. Drury[13], F. Dubois[11], G. Dubus[17], J. Dyks[24], M. Dyrda[28], K. Egberts[1,30], P. Eger[16], P. Espigat[12], L. Fallon[13], C. Farnier[15], S. Fegan[10], F. Feinstein[15], M. V. Fernandes[4], A. Fiasson[11], A. Förster[1], G. Fontaine[10], M. Füßling[5], S. Gabici[13], Y. A. Gallant[15], L. Gérard[12], D. Gerbig[21], B. Giebels[10], J. F. Glicenstein[7], B. Glück[16], P. Goret[7], D. Göring[16], D. Hampf[4], M. Hauser[14], S. Heinz[16], G. Heinzelmann[4], G. Henri[17], G. Hermann[1], J. A. Hinton[25], A. Hoffmann[18], W. Hofmann[1], P. Hofverberg[1], M. Holleran[9], S. Hoppe[1], D. Horns[4], A. Jacholkowska[19], O. C. de Jager[9], C. Jahn[16], I. Jung[16], K. Katarzyński[27], U. Katz[16], S. Kaufmann[14], M. Kerschhaggl[5], D. Khangulyan[1], B. Khélifi[10], D. Keogh[8], D. Klochkov[18], W. Kluźniak[24], T. Kneiske[4], Nu. Komin[7], K. Kosack[7], R. Kossakowski[11], G. Lamanna[11], J.-P. Lenain[6], T. Lohse[5], C.-C. Lu[1], V. Marandon[12], A. Marcowith[15], J. Masbou[11], D. Maurin[19], T. J. L. McComb[8], M. C. Medina[6], J. Méhault[15], R. Moderski[24], E. Moulin[7], M. Naumann-Godo[10], M. de Naurois[19], D. Nedbal[20], D. Nekrassov[1], N. Nguyen[4], B. Nicholas[26], J. Niemiec[28], S. J. Nolan[8], S. Ohm[1], J.-F. Olive[3], E. de Oña Wilhelmi[1], B. Opitz[4], K. J. Orford[8], M. Ostrowski[23], M. Panter[1], M. Paz Arribas[5], G. Pedaletti[14], G. Pelletier[17], P.-O. Petrucci[17], S. Pita[12], G. Pühlhofer[18], M. Punch[12], A. Quirrenbach[14], B. C. Raubenheimer[9], M. Raue[1,33], S. M. Rayner[8], O. Reimer[30], M. Renaud[12], R. de los Reyes[1], F. Rieger[1,33], J. Ripken[31], L. Rob[20], S. Rosier-Lees[11], G. Rowell[26], B. Rudak[24], C. B. Rulten[8], J. Ruppel[21], F. Ryde[32], V. Sahakian[2], A. Santangelo[18], R. Schlickeiser[21], F. M. Schöck[16], A. Schönwald[5], U. Schwanke[5], S. Schwarzburg[18], S. Schwemmer[14], A. Shalchi[21], I. Sushch[5], M. Sikora[24], J. L. Skilton[25], H. Sol[6], Ł. Stawarz[23], R. Steenkamp[22], C. Stegmann[16], F. Stinzing[16], A. Szostek[23,17], P. H. Tam[14], J.-P. Tavernet[19], R. Terrier[12], O. Tibolla[1], M. Tluczykont[4], K. Valerius[16], C. van Eldik[1], G. Vasileiadis[15], C. Venter[9], L. Venter[6], J. P. Vialle[11], A. Viana[7], P. Vincent[19], M. Vivier[7], H. J. Völk[1], F. Volpe[1], S. Vorobiov[15], S. J. Wagner[14], M. Ward[8], A. A. Zdziarski[24], A. Zech[6], and H.-S. Zechlin[4]

(Affiliations can be found after the references)

Received 25 February 2009 / Accepted 6 April 2010

ABSTRACT

Aims. The properties of the broad-band emission from the high-frequency peaked BL Lac H 2356–309 ($z = 0.165$) are investigated.
Methods. Very high energy (VHE; $E > 100$ GeV) observations of H 2356–309 were performed with the High Energy Stereoscopic System (HESS) from 2004 through 2007. Simultaneous optical/UV and X-ray observations were made with the XMM-Newton satellite on June 12/13 and June 14/15, 2005. NRT radio observations were also contemporaneously performed in 2005. ATOM optical monitoring observations were also made in 2007.
Results. A strong VHE signal, $\sim 13\sigma$ total, was detected by HESS after the four years HESS observations (116.8 h live time). The integral flux above 240 GeV is $I(>240\ \mathrm{GeV}) = (3.06 \pm 0.26_{\mathrm{stat}} \pm 0.61_{\mathrm{syst}}) \times 10^{-12}\ \mathrm{cm}^{-2}\,\mathrm{s}^{-1}$, corresponding to ~1.6% of the flux observed from the Crab Nebula. A time-averaged energy spectrum is measured from 200 GeV to 2 TeV and is characterized by a power law (photon index of $\Gamma = 3.06 \pm 0.15_{\mathrm{stat}} \pm 0.10_{\mathrm{syst}}$). Significant small-amplitude variations in the VHE flux from H 2356–309 are seen on time scales of months and years, but not on shorter time scales. No evidence for any variations in the VHE spectral slope are found within these data. The XMM-Newton X-ray measurements show a historically low X-ray state, characterized by a hard, broken-power-law spectrum on both nights.
Conclusions. The broad-band spectral energy distribution (SED) of the blazar can be adequately fit using a simple one-zone synchrotron self-Compton (SSC) model. In the SSC scenario, higher VHE fluxes could be expected in the future since the observed X-ray flux is at a historically low level.

Key words. galaxies: active – BL Lacertae objects: individual: H 2356–309 – gamma rays: galaxies

1. Introduction

H 2356–309 was suggested by Costamante & Ghisellini (2002) as a strong candidate for the detection of VHE emission, based on simple one-zone synchrotron self-Compton (SSC) modeling of its spectral energy distribution (SED). Motivated by

⋆ Supported by CAPES Foundation, Ministry of Education of Brazil.
⋆⋆ Now at Harvard-Smithsonian Center for Astrophysics, Cambridge, MA, USA.
⋆⋆⋆ Now at HEPL/KIPAC, Stanford University, Stanford, CA, USA.

these predictions, the HESS collaboration observed this blazar in 2004, resulting in the discovery of VHE γ-ray emission (Aharonian et al. 2006a). Although several blazars are known to have variable VHE γ-ray fluxes (see, e.g., Aharonian et al. 2007) and photon spectra (see, e.g., Aharonian et al. 2005), no strong evidence was found for such variability in the HESS data on this source from June through December 2004.

Hosted by an elliptical galaxy at a redshift of $z = 0.165$ (Falomo 1991), H 2356–309 is among the more distant blazars detected at VHE energies. As a result, its observed spectrum is expected to be strongly affected (softened) by the absorption of VHE photons on the extragalactic background light (EBL). The unexpectedly hard ($\Gamma \sim 3.1$) VHE spectrum measured by HESS in 2004 was used to confirm the strong constraints on the density of the EBL, near lower limits based on the integrated light of resolved galaxies (Aharonian et al. 2006a), given by the HESS spectrum from another VHE blazar (1ES 1101–232).

At X-ray energies, H 2356–309 was initially detected by the UHURU satellite (Forman et al. 1978) and later by the HEAO-I satellite (Wood et al. 1984). It is among the X-ray brightest of the 150 high-frequency peaked BL Lac objects (HBL) in the Sedentary Survey (Giommi et al. 2005), which contains HBLs characterized by their exceptionally high X-ray-to-radio flux ratio. BeppoSAX observations (Costamante et al. 2001) of H 2356–309 in June 1998 yielded an X-ray spectrum extending up to 50 keV, characterized by a broken power-law shape ($\Gamma_1 = 0.78^{+0.06}_{-0.07}$; $\Gamma_2 = 1.10 \pm 0.04$) with a break at 1.8 ± 0.4 keV. A softer power-law spectrum between 2 and 10 keV with an X-ray photon index of ($\Gamma_X = 2.43 \pm 0.11$) was measured (Aharonian et al. 2006b) during observations by the RXTE satellite on November 11, 2004. The RXTE spectrum is softer above 2 keV and the flux ($9.7^{+0.3}_{-1.3} \times 10^{-12}$ erg cm^{-2} s^{-1}) is ~3 times lower than that measured by BeppoSAX (2.5×10^{-11} erg cm^{-2} s^{-1}) in the same energy band.

The 2004 RXTE data were taken simultaneously with HESS VHE, ROTSE-IIIc optical, and Nancay radio-telescope observations. The double-peaked SED derived from this campaign (Aharonian et al. 2006b) was the first to include a contemporaneous VHE detection, and hence the first to sample the higher-energy SED peak for this object since H 2356–309 was not detected by the EGRET satellite. Modeling of these multi-wavelength observations demonstrated that the SED of H 2356–309 could be adequately fit by a simple one-zone stationary SSC scenario.

Results from 76.9 hrs of new HESS observations of H 2356–309 in 2005, 2006 and 2007 are reported here. In addition, a re-analysis of the previously published 2004 HESS data (39.9 h), with an improved calibration of the absolute energy scale of the detector, is presented. This improvement in the HESS calibration was not included in the previously mentioned modeling of the 2004 multi-wavelength observations, therefore this modeling is repeated. In addition, the XMM-Newton satellite simultaneously observed H 2356–309 on two nights (~5 h each night) at X-ray energies, as well as at optical through ultraviolet wavelengths, during the HESS observations in June 2005. The results from this multi-wavelength observation campaign, which has much improved X-ray and optical measurements, are also discussed.

2. HESS observations and analysis technique

From 2004 through 2007, a total of 175.3 h of HESS observations were taken on H 2356–309 in *wobble mode*, where the telescope tracking position is offset by ±0.5° in either right ascension or declination relative to the source location. After applying the standard HESS data-quality selection, the exposure is 116.8 h live time at a mean zenith angle of $Z_{\rm mean} = 19°$. The HESS data are calibrated following the procedures described in Aharonian et al. (2004). The analysis is performed using the standard HESS tools and γ-ray-like events are selected using the *standard cuts* (Benbow 2005; Aharonian et al. 2006c). The average post-analysis energy threshold[1] is 240 GeV at $Z_{\rm mean}$. The signal (on-source data) is taken from events with reconstructed direction falling within a circular region of radius $\theta_{\rm cut} = 0.11°$ centered on H 2356–309. The background (off-source data) is estimated using the *Reflected-Region* method (Berge et al. 2007), hence the on-source and off-source data are measured simultaneously from events in the same field of view. Equation (17) in Li & Ma (1983) is used to calculate the significance of any excess.

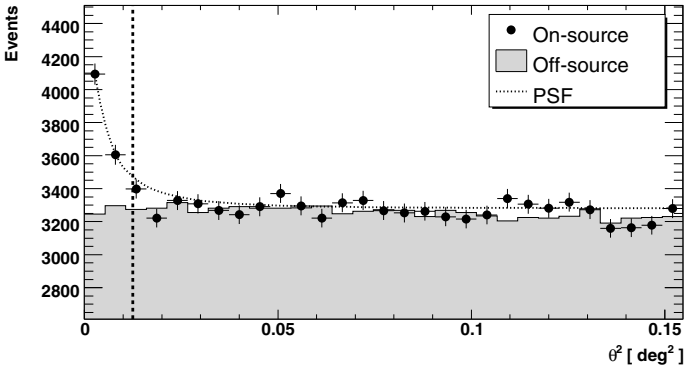

Fig. 1. Distribution of θ^2 for on-source events (points) and normalized off-source events (shaded) from observations of H 2356–309. The dashed curve represents the expected distribution for a VHE γ-ray point source with photon index $\Gamma = 3.06$ at a zenith angle of 20°. The vertical line denotes the on-source integration region relative to the nominal source position (Falomo 1991).

The optical throughput of HESS decreases over time due to degradation of the reflective surfaces of the HESS mirrors and Winston cones, as well as to the accumulation of dust on the optical elements. Compared to a newly-commissioned HESS telescope (mirror installation between October 2001 and August 2003), this decrease is on average ~26% for the entire data sample, and is 20%, 27%, 32% and 35% for the H 2356–309 data in 2004, 2005, 2006 and 2007, respectively. This decrease causes images from gamma rays of equivalent energy to appear less bright in later data, requiring a renormalization of the event energy. This normalization is made using the ratio of efficiencies determined from simulated and observed muons (Aharonian et al. 2006c), and eliminates long-term variations in the absolute energy scale of the HESS analysis due to a changing optical throughput.

3. HESS results

A total of 1185 excess events (12.6σ) is measured from the direction of H 2356–309 in the complete data set. Figure 1 shows the on-source and normalized off-source distributions of the square of the angular difference between the source position (Falomo 1991) and the reconstructed shower position (θ^2) for all observations. The observed signal can be seen at small values of

[1] The threshold is corrected to account for the decreased optical efficiency of the HESS mirrors over the observation period.

Table 1. Results from four years of HESS observations of H 2356–309.

Dark Period	MJD First	MJD Last	Time [h]	On	Off	α	Excess	Sig [σ]	I(>240 GeV)[a] [10^{-12} cm^{-2} s^{-1}]	Crab[b] %	χ^2, NDF[c]	$P(\chi^2)$[c]
06/2004	53 172	53 186	7.9	835	7778	0.0938	106	3.7	3.86 ± 0.88	2.1	8.9, 11	0.63
07/2004	53 201	53 209	3.0	280	2655	0.0938	31	1.8	1.19 ± 1.18	0.6	1.4, 4	0.84
09/2004	53 256	53 269	6.9	759	6015	0.0937	195	7.4	6.91 ± 0.94	3.7	4.0, 6	0.67
10/2004	53 286	53 296	9.9	950	8496	0.0914	174	5.7	4.33 ± 0.80	2.3	9.9, 6	0.13
11/2004	53 316	53 319	4.1	300	2700	0.0912	54	3.2	3.82 ± 1.22	2.0	7.0, 3	0.07
12/2004	53 341	53 353	8.2	559	5867	0.0926	16	0.6	1.23 ± 1.46	0.7	7.2, 5	0.21
06/2005	53 530	53 541	20.4	1200	12 275	0.0921	69	2.0	1.78 ± 1.04	1.0	6.3, 9	0.71
07/2005	53 556	53 570	16.5	1455	13 375	0.0922	221	5.9	3.08 ± 0.60	1.6	12.9, 13	0.46
08/2005	53 583	53 587	7.3	495	4920	0.0927	39	1.7	0.56 ± 0.85	0.3	5.7, 4	0.22
09/2005	53 614	53 615	2.6	152	1477	0.0946	12	1.0	2.70 ± 1.67	1.4	0.0, 1	0.96
07/2006	53 937	53 942	8.1	598	5926	0.0893	69	2.8	2.27 ± 0.89	1.2	2.5, 5	0.77
08/2006	53 970	53 978	2.2	188	1427	0.0894	60	4.8	7.39 ± 1.84	3.9	0.5, 3	0.91
09/2006	53 999	54 005	12.9	626	6044	0.0931	64	2.7	1.26 ± 0.77	0.7	7.2, 6	0.30
07/2007	54 295	54 307	7.0	502	4670	0.0915	75	3.4	3.48 ± 1.07	1.9	8.9, 10	0.54
2004	53 172	53 353	39.9	3683	33 511	0.0927	576	9.6	4.06 ± 0.42	2.2	19.1, 5	0.002
2005	53 530	53 615	46.7	3302	32 047	0.0924	341	5.9	2.22 ± 0.44	1.2	6.1, 3	0.11
2006	53 937	54 005	23.2	1412	13 397	0.0910	193	5.1	2.36 ± 0.56	1.3	9.5, 2	0.01
2007	54 295	54 307	7.0	502	4670	0.0915	75	3.4	3.48 ± 1.07	1.9	–	–
Total	53 172	54 307	116.8	8899	83 625	0.0923	1185	12.6	3.06 ± 0.26	1.6	11.0, 3	0.01

Notes. [a] The 20% systematic error on the observed integral flux above 240 GeV is not shown. [b] The Crab nebula flux percentage is calculated relative to the HESS value above 240 GeV (Aharonian et al. 2006c). [c] The χ^2, degrees of freedom (NDF), and corresponding χ^2 probability $P(\chi^2)$ are given for fits of a constant to I(>240 GeV) binned nightly within a dark period, or monthly within a year, or yearly within the total.

θ^2 and the distribution of the excess is similar to that expected from a simulated γ-ray point source.

H 2356–309 is clearly detected with a statistical significance of more than 5 standard deviations (σ), in each of the first three years (2004-06) of HESS observations, and a marginal excess (3.4σ) is observed during the brief observations in 2007. Detailed results of the HESS observations of H 2356–309 for individual observation periods are summarized in Table 1. The table contains the dead-time-corrected observation time, the number of on and off-source events, the on/off normalization (α), the observed excess and its statistical significance for various intervals (e.g. dark periods) in which H 2356–309 was observed.

A two-dimensional Gaussian fit to the sky map of the observed excess demonstrates that the excess is point-like with an upper limit (99% confidence level) on the extension of 1.3′. The centroid of the fit, HESS J2359–306, is located at $\alpha_{J2000} = 23^h59^m7.8^s \pm 1.6^s_{stat} \pm 1.3^s_{syst}$ and $\delta_{J2000} = -30°37'18'' \pm 20''_{stat} \pm 20''_{syst}$. HESS J2359–306 is spatially consistent with the position (Falomo 1991) of the blazar ($\alpha_{J2000} = 23^h59^m7.8^s$, $\delta_{J2000} = -30°37'38''$) as expected. The distance between the two positions is $20'' \pm 31''$.

3.1. VHE spectrum of H 2356–309

Figure 2 shows the four-year (2004–2007) time-averaged photon spectrum of H 2356–309. The best χ^2 fit of a power law ($dN/dE = I_\circ(E/1\,\mathrm{TeV})^{-\Gamma}$) to these data yields a photon index $\Gamma = 3.06 \pm 0.15_{stat} \pm 0.10_{syst}$, and a χ^2 of 5.7 for 6 degrees of freedom. The last spectral point at ∼1.7 TeV is not significant (0.8σ), however removing it from the fit does not appreciably change the result. Fitting the observed photon spectrum with a more complex function, such as a power-law with a cutoff or

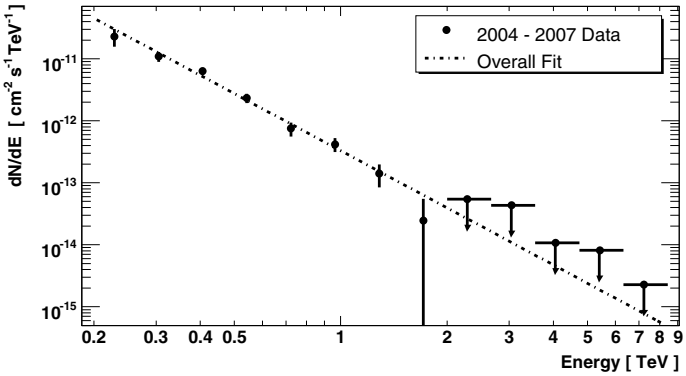

Fig. 2. Time-averaged (2004–2007) VHE photon spectrum of H 2356–309. The dashed line represents the best χ^2 fit of a power law to the data up to 2 TeV, and a linear extrapolation at higher energies. The upper limits are at the 99% confidence level (Feldman & Cousins 1998). Only the statistical errors are shown.

break, does not yield a χ^2 that is significantly improved (as determined by an F-test).

The high photon statistics observed in 2004, 2005 and 2006 enable the determination of a spectrum for each of those years. Unfortunately a spectrum could not be generated for the 2007 data due to low statistics. The annual spectra for the first three years of observations are shown in Fig. 3 together with the best χ^2 fit of a power law to the data. Table 2 gives the fit results for each of the annual spectra, as well as for the total spectrum. The epoch, lower and upper energy bounds, photon index (Γ), differential flux normalization at 1 TeV ($I_\circ$), χ^2, degrees of freedom (NDF), and χ^2 probability ($P(\chi^2)$) for each fit are shown. Although the differential flux normalization $I_\circ$ is ∼1.5 times

Table 2. Results of power-law fits to the VHE spectra of H 2356–309.

Epoch	E_{min} [TeV]	E_{max} [TeV]	Γ	I_o[a] [10^{-13} cm^{-2} s^{-1} TeV^{-1}]	χ^2	NDF	$P(\chi^2)$
2004 (AH06)[b]	0.165	1.041	$3.06 \pm 0.21_{stat} \pm 0.10_{syst}$	$3.08 \pm 0.75_{stat} \pm 0.62_{syst}$	3.9	6	0.69
2004[c]	0.200	1.500	$2.97 \pm 0.19_{stat} \pm 0.10_{syst}$	$4.69 \pm 0.86_{stat} \pm 0.94_{syst}$	7.8	5	0.17
2005	0.200	2.000	$2.99 \pm 0.39_{stat} \pm 0.10_{syst}$	$2.92 \pm 0.89_{stat} \pm 0.58_{syst}$	5.0	6	0.55
2006[d]	0.200	2.000	$3.43 \pm 0.41_{stat} \pm 0.10_{syst}$	$2.13 \pm 0.79_{stat} \pm 0.43_{syst}$	0.7	2	0.70
Total	0.200	2.000	$3.06 \pm 0.15_{stat} \pm 0.10_{syst}$	$3.29 \pm 0.45_{stat} \pm 0.66_{syst}$	5.7	6	0.47

Notes. [a] The differential flux normalization is calculated at 1 TeV. [b] The AH06 entry is the previously published HESS result (Aharonian et al. 2006a) for the 2004 data and is not corrected for long-term changes in the optical efficiency of the system. [c] This 2004 entry is derived from the exact same data as presented in AH06, but with a correction (see text) applied to account for the optical efficiency changes within the data. The 2005, 2006 and total entries also have this correction applied. [d] Due to low statistics, the 2006 spectrum is determined using 4 bins/decade in energy instead of the 8 bins/decade used for the other photon spectra.

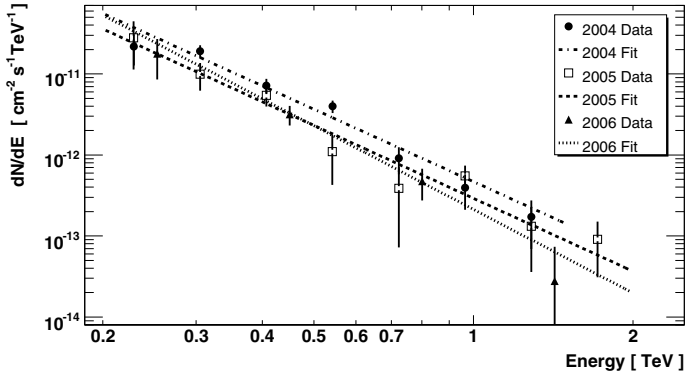

Fig. 3. Annual VHE photon spectra observed by HESS from H 2356–309. Each line represents the best χ^2 fit of a power law to the observed data. Only the statistical errors are shown.

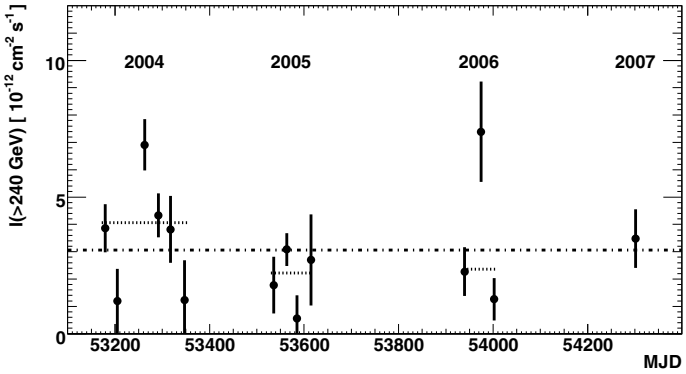

Fig. 4. Integral flux, I(>240 GeV), measured by HESS from H 2356–309 during each dark period of observations. For each point the time-averaged $\Gamma = 3.06$ is assumed and only the statistical errors are shown. The horizontal line represents the average flux for all the HESS observations. The three horizontal line segments are the average 2004, 2005 and 2006 fluxes.

larger in 2004 than in 2005 and 2006, there are no significant changes in the spectral slope during the HESS observations.

3.2. VHE flux from H 2356–309

The observed integral flux[2] above 240 GeV for the entire data set is $I(>240\ \mathrm{GeV}) = (3.06 \pm 0.26_{stat} \pm 0.61_{syst}) \times 10^{-12}$ cm^{-2} s^{-1}, corresponding to ~1.6% of I(>240 GeV) determined by HESS from the Crab Nebula (Aharonian et al. 2006c). Figures 4 and 5 show the flux measured for each dark period and night, respectively. The integral flux I(>240 GeV) for each year of observations, as well as for each dark period, is shown in Table 1. Also given are the χ^2 and corresponding probability for a fit of a constant to the data when binned by nights within each dark period, by dark periods within a year, and by year within the total observations. There are clear indications that the VHE flux from H 2356–309 varies weakly on time scales of months and years. There is no evidence for flux variability on any shorter time scale within the HESS data, however the average flux is too low to significantly detect similar weak variations during such brief exposures.

3.3. Optical efficiency correction

The previously published (Aharonian et al. 2006a) spectrum of H 2356–309 in 2004 was not corrected for optical sensitivity changes. Figure 6 illustrates the effect of correcting the energy of individual events for the relative optical efficiency of the system. The results of the best fit to each set of points is shown in Table 2. As can be seen, the corrected spectrum has a significantly larger flux normalization (I_o), but the photon index (Γ) is unchanged. The corrected 2004 integral flux is ~50% higher than previously published. The increase in integral flux due to the optical efficiency correction is relatively large for H 2356–309 because of the softness of the observed VHE specrum. The correction is smaller for harder spectrum sources (e.g., typical Galactic VHE sources).

4. Multi-wavelength observations

The emission from blazars is known to span over twenty orders of magnitude in energy and is variable at all energies. Accurate modeling of the underlying processes in these objects thus requires simultaneous observations at many wavelengths. Two such simultaneous multi-wavelength observation campaigns were organized by the HESS collaboration for H 2356–309. The first of these included the RXTE X-ray satellite, the ROTSE-IIIc optical telescope and the Nancay Radio Telescope (NRT), and is henceforth referred to as the RXTE campaign. The second campaign involved X-ray and optical/UV observations with XMM-Newton satellite and further NRT data, and is henceforth referred to as the XMM-Newton campaign. In addition,

[2] All HESS fluxes (i.e. annual, dark period and nightly values) in this article are calculated using the time-averaged $\Gamma = 3.06$.

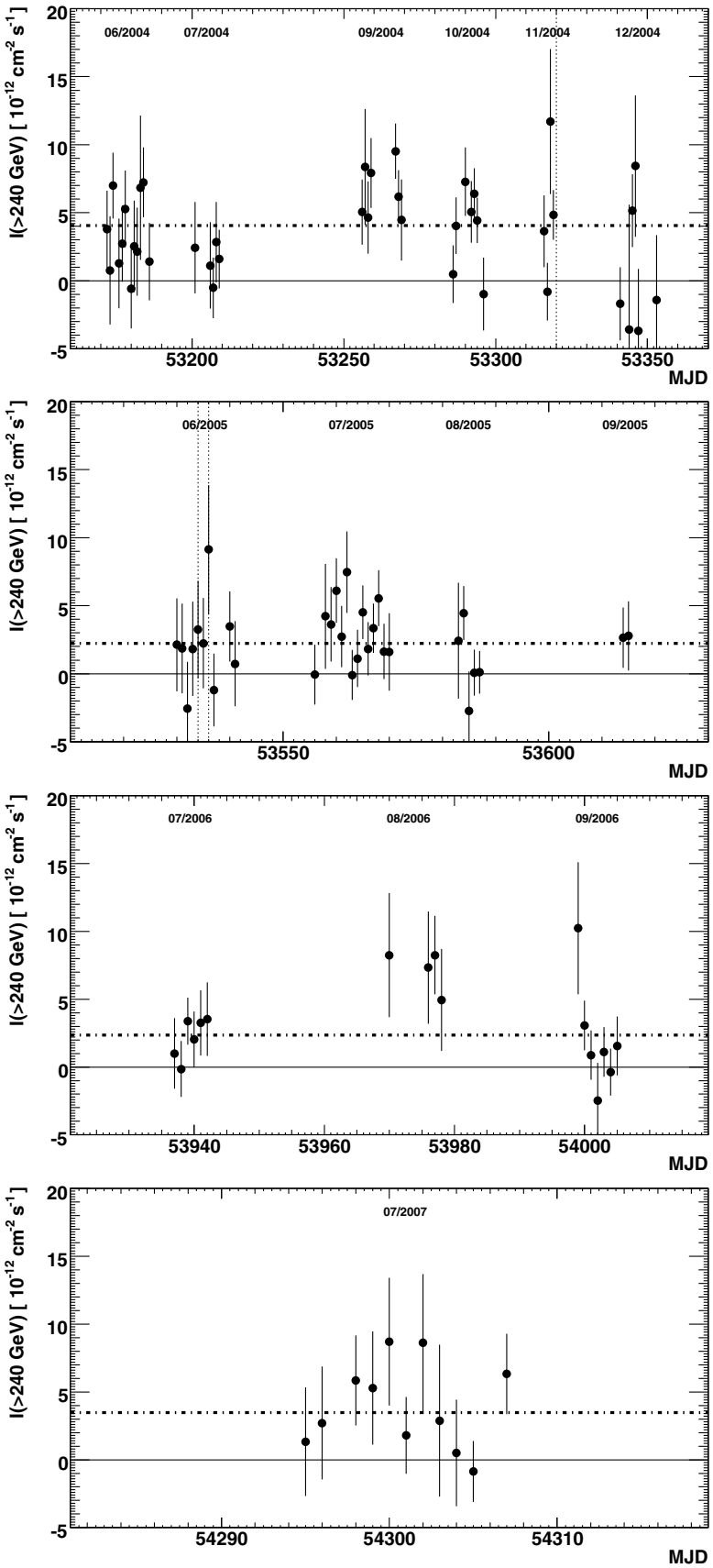

Fig. 5. Integral flux, $I(>240\ \mathrm{GeV})$, measured by HESS from H 2356–309 during each night of observations in 2004 (*top*), 2005 (*top-middle*), 2006 (*bottom-middle*) and 2007 (*bottom*). For each point the time-averaged $\Gamma = 3.06$ is assumed, and only the statistical errors are shown. The horizontal line in each figure represents the average flux measured by HESS in the respective year. The night of the RXTE observations (MJD 53 320) is denoted by the dotted vertical line in the 2004 light curve. The nights (MJD 53 534 and 53 536) of the XMM-Newton observations are marked by dotted vertical lines in the 2005 figure.

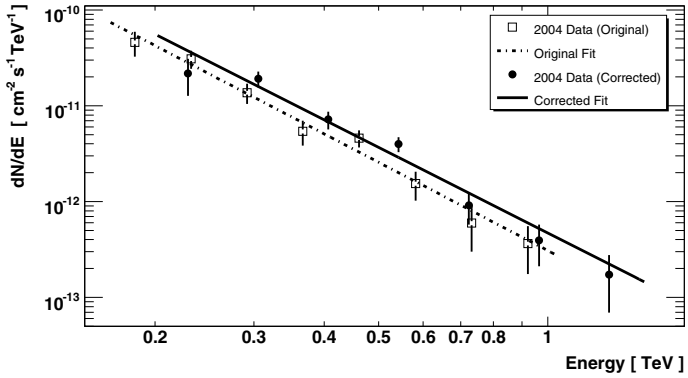

Fig. 6. Renormalized VHE spectrum measured by HESS from H 2356–309 in 2004 compared to the previously published version (Aharonian et al. 2006a). Only the statistical errors are shown.

results of ATOM optical monitoring of H 2356–309 beginning in November 2006 are presented.

4.1. RXTE campaign

Results from the RXTE campaign were first reported in Aharonian et al. (2006b). As only the normalization of the HESS observations have changed, the previously reported lower-frequency results are summarized here. The RXTE/PCA observed H 2356–309 for a total of 2.14 ks on November 11, 2004 (MJD 53320) as a target-of-opportunity request. The constant X-ray flux was $9.7^{+0.3}_{-1.3}\times10^{-12}$ erg cm^{-2} s^{-1} in the 2–10 keV band. The X-ray spectrum was generated by combining data from three separate PCUs, yielding a single-PCU equivalent exposure of 5.42 ks, and is compatible with a power-law function with photon index $\Gamma_X = 2.43 \pm 0.11$. The average NRT 11-cm flux between June 11 and October 10, 2004 was 40 ± 8 mJy. During the observations by HESS in 2004, ROTSE-IIIc measured apparent R-band magnitudes $m(R)$ between 16.1 and 16.9, with an estimated contribution from the resolved elliptical host galaxy of $m(R) = 17$. Due to poor weather, HESS was unable to observe the blazar on MJD 53 320. However, there is no evidence for variability in the November 2004 VHE flux and this flux is consistent with the average 2004 VHE flux. As there is no evidence for changes in the spectral slope of H 2356–309 on any time scale, the time-averaged VHE spectrum from 2004 is assumed to represent the VHE state of the blazar during the RXTE campaign for the SED modeling in Sect. 5. The same assumption was made in Aharonian et al. (2006b).

4.2. XMM-Newton campaign

The XMM-Newton satellite was pointed at H 2356–309 on two nights in 2005. The first XMM-Newton pointing began at 23:59 UTC on June 12, 2005 and ended at 5:17 UTC on June 13, 2005 (MJD 53 334). The second pointing started at 23:57 UTC on June 14, 2005 and finished at 5:19 UTC on June 15, 2005 (MJD 53 536). Simultaneous HESS observations of the blazar were also made during both of the XMM-Newton pointings. At radio wavelengths, the 11-cm flux from H 2356–309 was contemporaneously monitored by the NRT.

4.2.1. HESS results

The total HESS exposure during the XMM-Newton campaign is 4.68 h live time after selection criteria. The data are divided approximately evenly over the two nights with exposures of 2.44 h and 2.24 h on MJD 53 534 and 53 536, respectively. HESS did not detect a significant excess from H 2356–309 on either night of the XMM-Newton observations. During these two nights, a total of 302 on-source events and 2907 off-source events were measured with an on-off normalization of 0.0930, corresponding to an excess of 32 events (1.8σ). Due to the lack of a significant detection it is not possible to produce a photon spectrum from the data. Assuming the observed excess is from γ-rays emitted by H 2356–309, the average flux during the XMM-Newton observations, $I(>240\ \mathrm{GeV}) = (5.7 \pm 2.9_{\mathrm{stat}} \pm 1.1_{\mathrm{syst}}) \times 10^{-12}$ cm^{-2} s^{-1}, is consistent with time-averaged value from 2005. The flux for each of the nights (MJD 53 534 and 53 536) in the XMM-Newton epoch can be seen in Fig. 5. There are no significant variations of the nightly flux, or of the run-wise (~28 min) flux in either of the individual nights, during the XMM-Newton observations. Since there are no indications of any VHE flux variations in 2005, the time-averaged VHE spectrum from 2005 is used for the SED modeling of the each night of the XMM-Newton campaign in Sect. 5.

4.2.2. XMM-Newton X-ray results

During the two pointings, the XMM-Newton EPIC instruments were set in timing (PN and MOS1 cameras) and large window (MOS2 camera) modes. On MJD 53 534 the total live time of the XMM-Newton exposures are $T_{\mathrm{PN}} = 16.5$ ks for the EPIC PN instrument and $T_{\mathrm{MOS2}} = 17.6$ ks for the EPIC MOS2 detector. The live times are similar, $T_{\mathrm{PN}} = 16.6$ ks and $T_{\mathrm{MOS2}} = 17.7$ ks, on MJD 53 536. The XMM-Newton Science Analysis System (SAS version 7.1.0) is used to process the data with the July 2008 calibration files. The spectral and timing analysis are performed with `XSPEC v11.3.2ag` and `FTOOLS V6.3.2`. The MOS2 data are taken in Large Window mode, while the MOS1 in Timing mode. Data from the MOS1 detector are not included, as they are in qualitative agreement with the other instruments but exhibit much stronger noise levels. The 0.1–1 keV and 4–10 keV count rates of the PN, as well as the corresponding hardness ratio, are all constant in time on each of the two nights. Therefore only the night-averaged energy spectra are presented.

The effects of pile-up in the EPIC instruments were explored using `epatplot`. No significant pile-up is present. The spectrum is obtained by selecting only single pixel (`PATTERN=0`) events for the MOS2 data, and single plus double pixel events (`PATTERN≤4`) for the PN data.

For the MOS2 analysis, the signal is extracted from a circle of radius 45″ centered on the source centroid. The background is taken from an annulus around the source with an inner radius of 120″ and an outer radius set by the border of the CCD window. For the PN analysis, signal photons are selected from rows 28 ≤ RAWX ≤ 48 and the background is estimated from 2 ≤ RAWX ≤ 18. The energy range of the PN is restricted to 0.5 to 10 keV, while MOS2 events between 0.15 and 10 keV are accepted. For the spectral determination, different re-binning schemes are used, always requiring at least 50 counts per new bin. Ancillary and response files are produced with `rmfgen` and `arfgen`.

The spectra of the PN and MOS2 detectors are combined in the following fitting, with a free constant (that remained within a few percent of unity) to allow for the different normalization between the two instruments. The spectra are fit with source models including Galactic absorption along the line of sight to H 2356–309. The absorption model `TBabs` by Wilms et al. (2000) is used, with cross-sections by

Table 3. Spectral information from X-ray observations of H 2356–309.

Instrument	MJD	Model	Γ_1	$E_{\rm break}$ [keV]	Γ_2	$F_{0.1-2.0\ \rm keV}$ [10^{-12} erg cm^{-2} s^{-1}]^b	$F_{2-10\ \rm keV}$	$\chi^2_{\rm r}$, NDF^a
BeppoSAX	51 350–51	BPL	$0.78^{+0.06}_{-0.07}$	1.8 ± 0.4	1.10 ± 0.04	–	25	–
RXTE	53 320	PL	2.43 ± 0.25	–	–	–	$9.70^{+0.3}_{-1.3}$	–
XMM-Newton^c	53 534	PL	2.23 ± 0.01	–	–	25.9	8.05	1.41, 541
		BPL	2.08 ± 0.03	1.00 ± 0.08	2.32 ± 0.02	23.2	7.46	0.95, 539
XMM-Newton^c	53 536	PL	2.16 ± 0.01	–	–	25.9	9.54	1.52, 541
		BPL	1.89 ± 0.10	0.66 ± 0.14	2.20 ± 0.02	22.3	9.15	1.21, 539

Notes. ^{a} The reduced $\chi^2_{\rm r}$ and degrees of freedom (NDF) correspond to fits of either a power-law (PL) function or broken power-law (BPL) function to the XMM-Newton X-ray data.^{b} The integrated fluxes have the effects of Galactic absorption removed.^{c} All errors from the XMM-Newton fits are quoted at the 90% confidence level.

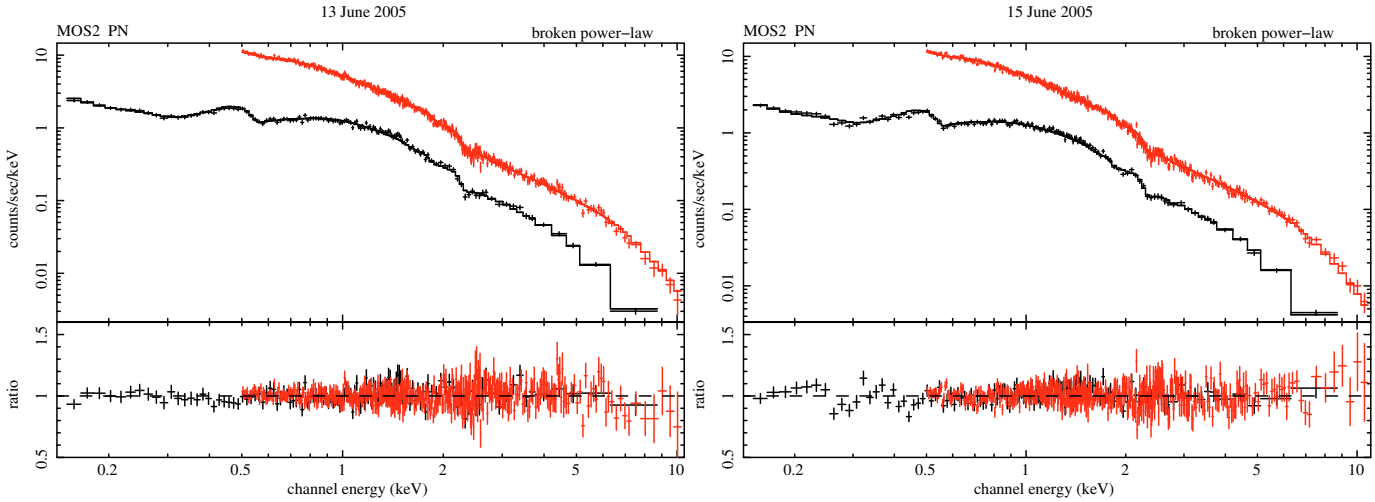

Fig. 7. X-ray spectra measured during the XMM-Newton observations in 2005. The *lefthand and righthand* figures correspond to the measurements on MJD 53 534 and 53 536, respectively. The red points (0.5 to 10 keV) and black points (0.15 to 10 keV) are data from the PN and MOS2 detectors, repectively. The corresponding fits to the data are also shown as lines, and the fit residuals are shown in the lower panels.

Verner et al. (1996). The absorbing column density is kept fixed at the Galactic value of $N_{\rm H} = 1.44 \times 10^{20}$ cm^{-2} (Kalberla et al. 2005).

A single power-law model does not provide an acceptable fit to the X-ray data of either night (see Table 3). Different models of the Galactic absorption (`wabs`, `phabs`) were also tested, but none of them provide an acceptable fit for a single power-law source model. A broken power-law provides an improved fit on both nights (F-test >99.999%), and also with respect to a fit with free $N_{\rm H}$ (reduced $\chi^2_{\rm r} = 0.95$ for 539 NDF vs. $\chi^2_{\rm r} = 1.12$ for 540 NDF).

The results of the broken power-law fits for both nights are shown in Table 3, along with a summary of archival X-ray spectrum measurements. The measured X-ray spectra for the XMM-Newton pointings on MJD 53 534 and 53 536 are shown in Fig. 7.

4.2.3. XMM-Newton optical monitor results

During the two pointings the XMM-Newton optical monitor (OM) took four exposures with four different filters ($V, B, U, UVW1$). For each exposure, the window on the target was set in fast mode. The XMM-Newton OM data are processed with `xmmsas 7.1.0` using data from the imaging mode for the photometry, and from the fast timing window for the light curves. No variability is found in any of the OM exposures for each of the different filters. The point-source analysis of the OM photometry program `omsource` is used to extract count rates, which are converted into fluxes following the standard procedures. For the V, B, and U filters, the on-source data are taken from an aperture of $R = 6''$ and the background is estimated from an annulus with $10'' < R < 15''$. An on-source aperture of $R = 17\farcs5$ and background annulus of $20'' < R < 25''$ are used for the UVW1 filter. Consistent results were also obtained using different background regions.

The optical spectrum for each of the two nights is generated by combining the results from all four filters. Each of the V and B band exposures of H 2356–309 contains a significant contribution from the host galaxy that must be subtracted. The host galaxy is resolved at optical (Falomo 1991; Scarpa et al. 2000) and near-infrared (Cheung et al. 2003) wavelengths, and is a normal elliptical galaxy with an effective radius of about $1\farcs7$ in the V and R bands, somewhat lower in the IR. Using a standard de Vaucouleurs radial profile, more than 60% of the host-galaxy flux is thus estimated to be contained in the V and B band signal apertures. The host-galaxy contribution to the background apertures is negligible. These fractions of the host galaxy flux are subtracted from the V and B band fluxes using the R band magnitude ($m_{\rm R} = 17.21$) from Urry et al. (2000), and the spectral template of elliptical galaxies ($z = 2$) from Fukugita et al. (1995).

Table 4. XMM-Newton optical monitor results.

Band	T_1[a] [ks]	F_1 [mJy]	T_2[a] [ks]	F_2 [mJy]
V	4.3	0.33	3.8	0.32
B	3.9	0.22	4.3	0.21
U	3.9	0.24	4.3	0.23
$UVW1$	4.4	0.24	4.4	0.23

Notes. [(a)] The OM exposures (T) and fluxes (F) are reported for each filter on MJD 53 534 (T_1 & F_1) and 53 536 (T_2 & F_2).

The host-galaxy-subtracted fluxes are corrected for Galactic extinction using $A_B = 0.058$ mag and the interstellar reddening curve by Cardelli et al. (1989), updated by O'Donnell (1994). The exposure (T) and observed flux (F) in each optical band are shown in Table 4 for each of the two nights. The contribution of the host galaxy to the other filters is negligible.

4.2.4. NRT results

The NRT (Theureau et al. 2007), a meridian transit telescope with a main spherical mirror of 300 m × 35 m, measured the 11-cm flux from H 2356–309 on 29 different days between June through December 2005 as part of an on-going monitoring program. The nearest observations to the XMM-Newton pointings were performed on the three nights of June 11–13, 2005. The observed 11-cm flux was quite low and not strongly variable during 2005, with an average of 7.5 ± 2.0 mJy.

4.3. ATOM results

Optical observations were taken using the ATOM telescope (Hauser et al. 2004) at the HESS site from November 2006 on. Absolute flux values are calculated using differential photometry against several stars listed in the NOMAD catalog (Zacharias et al. 2005). A 4 arcsec radius aperture is used for all filter bands. A total of ~500 measurements in 4 filter bands were taken between November 2006 and the end of 2007. The measured apparent magnitudes vary in the R band around (16.4 ± 0.2) mag. For the other filter bands, the values are (17.1 ± 0.2) mag in B, (17.0 ± 0.2) mag in V and (16.1 ± 0.2) mag in I band.

5. Discussion

The broad-band SED of H 2356–309 is shown in Figs. 8 and 9 for the RXTE campaign in 2004 and for each of the two XMM-Newton observations in 2005. All of these SEDs have the same shape as most VHE HBL, indicating a double-peaked structure with a roughly similar energy output in both the keV and VHE range. It should be noted that the optical, X-ray and VHE measurements from each of the three campaigns (RXTE, XMM-Newton on MJD 53534 and XMM-Newton on MJD 53 536) are very similar. The measured X-ray flux from 2 to 10 keV differs by only ±15% from the mean value, and the X-ray spectral slopes are consistent above 2 keV. The annual VHE fluxes differ by less than ±30% from the mean and the annual photon indexes are constant in time. As the VHE and X-ray spectral slopes are all consistent, and only modest changes in the VHE and X-ray fluxes are observed, it is expected that modeling of each of the three SEDs will result in similar physical parameters.

The aforementioned characterization of these three SEDs is performed using a simple, time-independent SSC model (Katarzyński et al. 2001). In this SSC scenario, the optical through VHE emission is generated by a spherical emission region of radius R relativistically propagating with a Doppler factor δ with respect to the observer through a homogeneous magnetic field B. The emission region is filled with relativistic electrons that generate the lower-energy peak at X-ray frequencies via synchrotron radiation and the higher-energy peak at VHE frequencies through inverse-Compton scattering of the synchrotron photons off the same electrons. The high-energy electron distribution between Lorentz factors $\gamma_{\rm min}$ and $\gamma_{\rm max}$ is assumed to have a broken power-law shape with normalization K and break $\gamma_{\rm b}$. The energy index of the electrons is n_1 below $\gamma_{\rm b}$, and n_2 above $\gamma_{\rm b}$. A low-energy cutoff in the electron distribution of $\gamma_{\rm min} = 1000$, is chosen to prevent an increase of the inverse-Compton emission in the MeV-GeV domain, that is not compatible with the non-contemporaneous upper limit on the blazar's MeV-GeV flux derived from the first 5.5 months of Fermi-LAT data (Abdo et al. 2009b). The majority of the radio emission is assumed to be produced from regions further out in the jet from the core. Therefore the NRT radio measurements are not used in the following SED modeling of the blazar, but can be considered as upper limits for the blazar's radio flux.

As H 2356–309 has a redshift of $z = 0.165$, its observed VHE spectrum is strongly affected by the absorption of VHE photons on the EBL (see, e.g., the review of Aharonian 2001). These interactions ($\gamma_{\rm VHE}\,\gamma_{\rm EBL} \rightarrow {\rm e}^+\,{\rm e}^-$; Gould & Schréder 1967) along the line-of-sight create an energy-dependent opacity $\tau(z, E)$ that is imprinted on the observed VHE spectrum ($F_{\rm obs}(E) = F_{\rm int}(E)\,{\rm e}^{-\tau(z,E)}$). To remove this absorption in the SED modeling the EBL density of Franceschini (2008) is used to calculate the optical depths relevant for these observations of H 2356–309. Fitting the de-absorbed time-averaged VHE spectrum to a power-law function ($dN/dE \sim E^{-\Gamma_{\rm int}}$) yields a relatively hard intrinsic photon index of $\Gamma_{\rm int} = 1.97 \pm 0.15$. Similar values of $\Gamma_{\rm int}$ are found when fitting the de-absorbed data from the 2004 and 2005 VHE spectra used in the SSC modeling. It should be noted that the approximate slope of each of the de-absorbed SSC curves (dashed lines in Figs. 8 and 9) is slightly steeper than the power-law fit to only the HESS EBL-de-absorbed data. This is due to the inclusion of all multi-wavelength data in the curved SSC fits, whereas the power-law function is fit to only the HESS data.

The parameters of the SSC fit to the SED from each of the XMM-Newton campaigns are shown in Table 5. For the modeling of the RXTE campaign, the XMM-Newton optical spectrum from MJD 53536 is used instead of the average ROTSE-IIIc flux from the 2004 season, since they are consistent and the former more strongly constrains the fit. In addition, the ROSTE-IIIc R-band measurement is modeled from white light, whereas the XMM OM data are from filtered light and hence are more appropriate for SED modeling. The data from the RXTE campaign are well described by the parameters of the SSC fit to the data from the second XMM-Newton night (MJD 53 536) and modification of these parameters does not yield an improved χ^2. Indeed the fit parameters do not vary greatly between the three campaigns, as expected from the similarity of the measured quantities. This may suggest that a steady state of the blazar was observed, and that this state can be explained by an SSC scenario. The slight hardening of the XMM-Newton spectrum between MJD 53 534 and 53 536 is easily accounted for by only a minor variation in the high-energy index of the electron distribution.

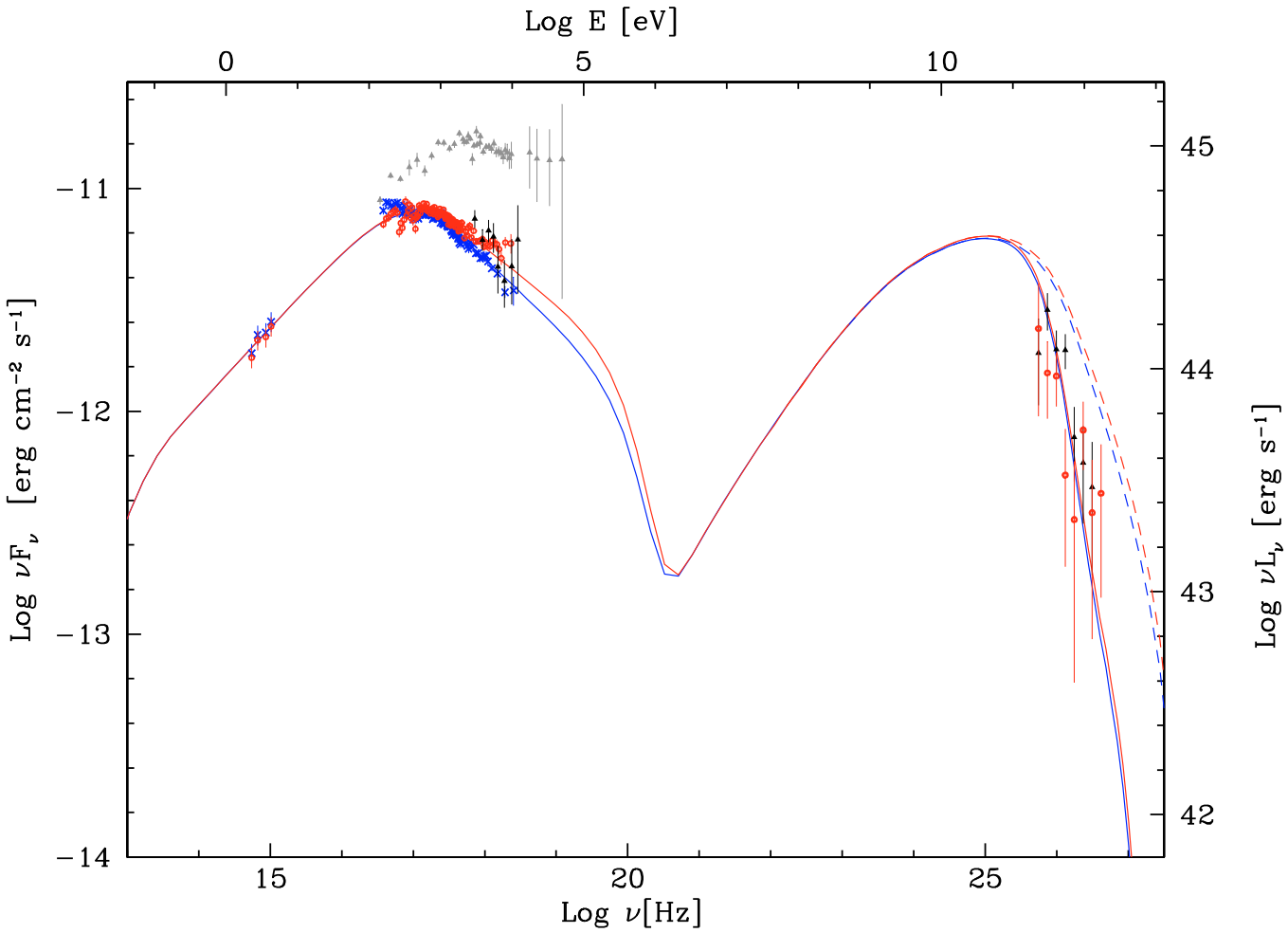

Fig. 8. SED of H 2356–309 in different epochs. The black triangles represent the SED from the 2004 RXTE campaign. The closed-blue and open-red circles represent the SED from the 2005 XMM-Newton observations on MJD 53 534 and 53 536, respectively. The light-gray triangles correspond to the BeppoSAX X-ray data during the high state observed in June 1998 (Costamante et al. 2001). In the *VHE* band, the black triangles and red circles are the time-average spectra observed in 2004 and 2005, respectively, and are not corrected for the effects of EBL absorption. The curves are fits to the respective SEDs of a single-zone homogeneous SSC model described in the text. The solid and dashed curves represent the same model with and without, respectively, the EBL effects included (Franceschini 2008). The SSC model fit to the 2004 RXTE campaign data is identical to the fit to the MJD 53 536 data (red curve). H 2356-309 does not appear in the Fermi-LAT bright-AGN list (Abdo et al. 2009a), and only poorly-constrained, non-simultaneous spectral data exist in the first Fermi-LAT catalog (Abdo et al. 2010). The NRT (11 cm) measurement falls well below the minimum flux density of the figure and is not shown for the sake of clarity. For the luminosity axis, the measured redshift of $z = 0.165$ is used with $H = 70$ km s^{-1} Mpc^{-1}, $\Omega_M = 0.3$.

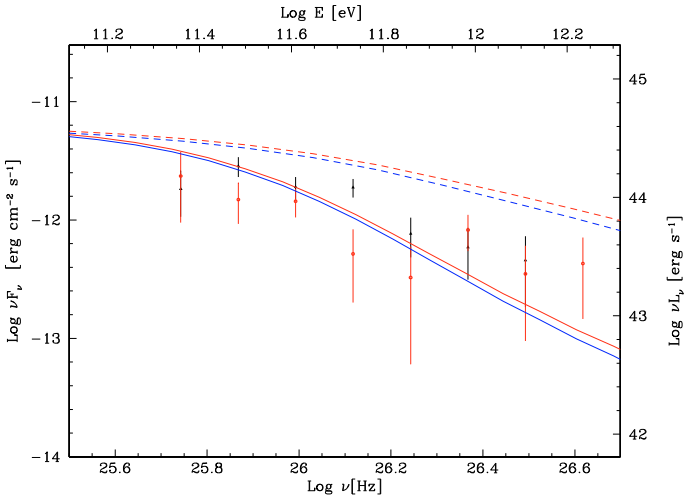

Fig. 9. SED of H 2356-309 zoomed in on the VHE band. The data and model curves are identical to those in Fig. 8.

It should also be noted that the parameters of the SSC fits indicate a cooling time scale of $\sim 1.5 \times 10^5$ s (~4 h), which is comparable to the source crossing time ($t_{esc} = R/c = 2.5 \times 10^5$ s), but is considerably shorter than the monthly time scale of the weak variations observed in the VHE band. However, VHE flux variations on time scales comparable to the cooling time (e.g. daily), and of approximately the same magnitude, cannot be ruled out due to the low average VHE flux.

The comparison of the results of the fits to the RXTE campaign in 2004 (see XMM_2 in Table 5) to the previously published results (Aharonian et al. 2006b) shows some differences. These differences are not primarily due to the renormalization (~50% increase) of HESS flux from this epoch. Rather they are largely due to the improved knowledge of the optical spectrum of the blazar from the XMM-Newton OM results. Using the ROTSE-IIIc flux instead of the XMM-Newton OM spectrum results in a different set of fit parameters (see RXTE† in Table 5), very similar to the previous modeling (see AH06 in Table 5). However, this fit (RXTE†) falls significantly below the measured

Table 5. Results of SSC fits to the SED of H 2356–309.

	XMM_1 [a]	XMM_2 [a]	RXTE†	AH06 [c]
δ	18	18	18	18
B [G]	0.16	0.16	0.16	0.16
R [cm]	7.5×10^{15}	7.5×10^{15}	7.0×10^{15}	3.4×10^{15}
K [cm^{-3}]	8.0×10^{4}	8.0×10^{4}	2.0×10^{4}	1.2×10^{4}
$\gamma_{\rm min}$	1.0×10^{3}	1.0×10^{3}	1.0×10^{3}	1.0×10^{3}
$\gamma_{\rm b}$	1.0×10^{5}	1.0×10^{5}	2.5×10^{5}	2.5×10^{5}
$\gamma_{\rm max}$	3.0×10^{6}	3.0×10^{6}	3.0×10^{6}	3.0×10^{6}
n_1	2.3	2.3	2.0	2.0
n_2	3.6	3.5	3.4	4.0

Notes. [(a)] The XMM_1 and XMM_2 results refer to the fits to the data from MJD 53 534 and 53 536, respectively. Using the XMM-Newton optical spectrum from MJD 53 536 instead of the average ROTSE-IIIc flux from 2004 for the RXTE campaign yields the same SSC fit parameters as shown in XMM_2. [(b)] This is the result of the original SSC modeling of the RXTE campaign SED of H 2356–309 published in Aharonian et al. 2006b. The RXTE† results use the same multi-wavelength data as AH06 along with an improved calibration of the VHE data.

XMM-Newton optical spectrum. As the optical portion of the SED is not expected to change dramatically, the characterization presented here (XMM_2) should be used as a reference for future studies.

6. Conclusion

Long term HESS observations of H 2356–309 have clearly confirmed the initial VHE detection from 2004. The source has a relatively low VHE flux (1.6% Crab) that is weakly variable (factor of ∼2) on time scales of at least months. Although the flux is variable, no changes in the VHE spectral slope ($\Gamma \approx 3.1$) are found. After accounting for the effects of the absorption of VHE photons on the extragalactic background light, the intrinsic VHE spectrum of H 2356–309 is found to be hard ($\Gamma_{\rm int} \approx 2.0$). Interestingly, the X-ray spectrum is also very hard, with the synchrotron peak located at ∼1 keV, despite the source being in a historically low state in X-rays. While the synchrotron peak of H 2356–309 is located at higher than typical energies and the X-ray and VHE spectra are comparatively hard, the SED can be reasonably modeled using a simple one-zone SSC scenario. This could be expected since the luminosity of both SED peaks are similar, and their separation in frequency is not extreme.

Acknowledgements. The support of the Namibian authorities and of the University of Namibia in facilitating the construction and operation of HESS is gratefully acknowledged, as is the support by the German Ministry for Education and Research (BMBF), the Max Planck Society, the French Ministry for Research, the CNRS-IN2P3 and the Astroparticle Interdisciplinary Programme of the CNRS, the U.K. Science and Technology Facilities Council (STFC), the IPNP of the Charles University, the Polish Ministry of Science and Higher Education, the South African Department of Science and Technology and National Research Foundation, and by the University of Namibia. We appreciate the excellent work of the technical support staff in Berlin, Durham, Hamburg, Heidelberg, Palaiseau, Paris, Saclay, and in Namibia in the construction and operation of the equipment.

References

Abdo, A. A., Ackermann, M., Ajello, M., et al. 2009a, ApJ, 700, 597
Abdo, A. A., Ackermann, M., Ajello, M., et al. 2009b, ApJ, 707, 1310
Abdo, A. A., Ackermann, M., Ajello, M., et al. 2010, ApJS, 188, 405
Aharonian, F. 2001, in Proc. 27th ICRC (Hamburg), ed. R. Schlickeiser, 250
Aharonian, F., Akhperjanian, A. G., Aye, K.-M., et al. (HESS Collaboration) 2004, Astropart. Phys., 22, 109
Aharonian, F., Akhperjanian, A. G., Aye, K.-M., et al. (HESS Collaboration) 2005, A&A, 437, 95
Aharonian, F., Akhperjanian, A. G., Bazer-Bachi, A. R., et al. (HESS Collaboration) 2006a, Nature, 440, 1018
Aharonian, F., Akhperjanian, A. G., Bazer-Bachi, A. R., et al. (HESS Collaboration) 2006b, A&A, 455, 461
Aharonian, F., Akhperjanian, A. G., Bazer-Bachi, A. R., et al. (HESS Collaboration) 2006c, A&A, 457, 899
Aharonian, F., Akhperjanian, A. G., Bazer-Bachi, A. R., et al. (HESS Collaboration) 2007, ApJ, 664, L71
Benbow, W. 2005, Proceedings of Towards a Network of Atmospheric Cherenkov Detectors VII (Palaiseau), 163
Berge, D., Funk, S., & Hinton, J. 2007, A&A, 466, 1219
Cardelli, J. A., Clayton, G. C., & Mathis, J. S. 1989, ApJ, 345, 245
Cheung, C. C., Urry, C. M., Scarpa, R., & Giavalisco, M. 2003, ApJ, 599, 155
Costamante, L., & Ghisellini, G. 2002, A&A, 384, 56
Costamante, L., Ghisellini, G., Giommi, P., et al. 2001, A&A, 371, 512
Falomo, R. 1991, AJ, 101, 821
Fazio, G. G., Ashby, M. L. N., Barmby, P., et al. 2004, ApJS, 154, 39
Feldman, G. J., & Cousins, R. D. 1998, Phys. Rev. D, 57, 3873
Forman, W., Jones, C., Cominsky, L., et al. 1978, ApJS, 38, 357
Franceschini, A., Rodighiero, G., & Vaccari, M. 2008, A&A, 487, 837
Fukugita, M., Shimasaku, K., & Ichikawa, T. 1995, PASP, 107, 945
Giommi, P., Piranomonte, S., Perri, M., & Padovani, P. 2005, A&A, 434, 385
Gould, R. J., & Schréder, G. P. 1967, Phys. Rev., 155, 1408
Hauser, M., Möllenhoff, C., Pühlhofer, G., et al. 2004, Astron. Nachr., 325, 659
Kalberla, P. M. W., Burton, W. B., Hartmann, D., et al. 2005, A&A, 440, 775
Katarzyński, K., Sol, H., & Kus, A. 2001, A&A, 367, 809
Li, T., & Ma, Y. 1983, ApJ, 272, 317
O'Donnell, J. E. 1994, ApJ, 422, 158
Primack, J. R., Bullock, J. S., & Somerville, R. S. 2005, AIP Conf. Proc., 745, 23
Scarpa, R., Urry, C. M., Padovani, P., Calzetti, D., & O'Dowd, M. 2000, ApJ, 544, 258
Theureau, G., Hanski, M. O., Coudreau, N., Hallet, N., & Martin, J.-M. 2007, A&A, 465, 71
Urry, C. M., Scarpa, R., O'Dowd, M., et al. 2000, ApJ, 532, 816
Verner, D. A., Ferland, G. J., Korista, K. T., & Yakovlev, D. G. 1996, ApJ, 465, 487
Wilms, J., Allen, A., & McCray, R. 2000, ApJ, 542, 914
Wood, K. S., Meekins, J. F., Yentis, D. J., et al. 1984, ApJS, 56, 507
Zacharias, N., Monet, D. G., Levine., S., et al. 2005, VizieR Online Data Catalog, 1297

[1] Max-Planck-Institut für Kernphysik, PO Box 103980, 69029 Heidelberg, Germany
e-mail: wbenbow@cfa.harvard.edu
[2] Yerevan Physics Institute, 2 Alikhanian Brothers St., 375036 Yerevan, Armenia
[3] Centre d'Étude Spatiale des Rayonnements, CNRS/UPS, 9 av. du Colonel Roche, BP 4346, 31029 Toulouse Cedex 4, France
[4] Universität Hamburg, Institut für Experimentalphysik, Luruper Chaussee 149, 22761 Hamburg, Germany
[5] Institut für Physik, Humboldt-Universität zu Berlin, Newtonstr. 15, 12489 Berlin, Germany
[6] LUTH, Observatoire de Paris, CNRS, Université Paris Diderot, 5 lace Jules Janssen, 92190 Meudon, France
e-mail: catherine.boisson@obspm.fr
[7] CEA Saclay, DSM/IRFU, 91191 Gif-Sur-Yvette Cedex, France
[8] University of Durham, Department of Physics, South Road, Durham DH1 3LE, UK
[9] Unit for Space Physics, North-West University, Potchefstroom 2520, South Africa
[10] Laboratoire Leprince-Ringuet, École Polytechnique, CNRS/IN2P3, 91128 Palaiseau, France
[11] Laboratoire d'Annecy-le-Vieux de Physique des Particules, Université de Savoie, CNRS/IN2P3, 74941 Annecy-le-Vieux, France
[12] Astroparticule et Cosmologie (APC), CNRS, Université Paris 7 Denis Diderot, 10 rue Alice Domon et Léonie Duquet, 75205 Paris Cedex 13, France; UMR 7164 (CNRS, Université Paris VII, CEA, Observatoire de Paris), France

[13] Dublin Institute for Advanced Studies, 5 Merrion Square, Dublin 2, Ireland
[14] Landessternwarte, Universität Heidelberg, Königstuhl, 69117 Heidelberg, Germany
[15] Laboratoire de Physique Théorique et Astroparticules, Université Montpellier 2, CNRS/IN2P3, CC 70, Place Eugène Bataillon, 34095 Montpellier Cedex 5, France
[16] Universität Erlangen-Nürnberg, Physikalisches Institut, Erwin-Rommel-Str. 1, 91058 Erlangen, Germany
[17] Laboratoire d'Astrophysique de Grenoble, INSU/CNRS, Université Joseph Fourier, BP 53, 38041 Grenoble Cedex 9, France
[18] Institut für Astronomie und Astrophysik, Universität Tübingen, Sand 1, 72076 Tübingen, Germany
[19] LPNHE, Université Pierre et Marie Curie Paris 6, Université Denis Diderot Paris 7, CNRS/IN2P3, 4 lace Jussieu, 75252 Paris Cedex 5, France
[20] Charles University, Faculty of Mathematics and Physics, Institute of Particle and Nuclear Physics, V Holešovičkách 2, 180 00 Prague 8, Czech Republic
[21] Institut für Theoretische Physik, Lehrstuhl IV: Weltraum und Astrophysik, Ruhr-Universität Bochum, 44780 Bochum, Germany
[22] University of Namibia, Department of Physics, Private Bag 13301, Windhoek, Namibia
[23] Obserwatorium Astronomiczne, Uniwersytet Jagielloński, ul. Orla 171, 30-244 Kraków, Poland
[24] Nicolaus Copernicus Astronomical Center, ul. Bartycka 18, 00-716 Warsaw, Poland
[25] School of Physics & Astronomy, University of Leeds, Leeds LS2 9JT, UK
[26] School of Chemistry & Physics, University of Adelaide, Adelaide 5005, Australia
[27] Toruń Centre for Astronomy, Nicolaus Copernicus University, ul. Gagarina 11, 87-100 Toruń, Poland
[28] Instytut Fizyki Jądrowej PAN, ul. Radzikowskiego 152, 31-342 Kraków, Poland
[29] Astronomical Observatory, The University of Warsaw, Al. Ujazdowskie 4, 00-478 Warsaw, Poland
[30] Institut für Astro- und Teilchenphysik, Leopold-Franzens-Universität Innsbruck, 6020 Innsbruck, Austria
[31] Oskar Klein Centre, Department of Physics, Stockholm University, Albanova University Center, 10691 Stockholm, Sweden
[32] Oskar Klein Centre, Department of Physics, Royal Institute of Technology (KTH), Albanova, 10691 Stockholm, Sweden
[33] European Associated Laboratory for Gamma-Ray Astronomy, jointly supported by CNRS and MPG